

Supervised versus unsupervised learning: approaching optimal memory retrieval in Hopfield networks

Marco Benedetti,^{1,*} Enrico Ventura,^{1,2,*} Enzo Marinari,^{1,†} Giancarlo Ruocco,^{1,†} and Francesco Zamponi^{2,†}

¹*Dipartimento di Fisica, Sapienza Università di Roma, P.le A. Moro 2, 00185 Roma, Italy*

²*Laboratoire de Physique de l'Ecole Normale Supérieure, ENS, Université PSL,
CNRS, Sorbonne Université, Université de Paris, F-75005 Paris, France*

(Dated: January 2, 2024)

The Hebbian unlearning algorithm, i.e. an unsupervised local procedure used to improve the retrieval properties in Hopfield-like neural networks, is numerically compared to a supervised algorithm to train a linear symmetric perceptron. We analyze the stability of the stored memories, which naturally maps the problem into a constraint satisfaction problem. Basins of attraction obtained by the Hebbian unlearning technique are found to be comparable in size to those obtained in the symmetric perceptron, while the two algorithms are found to converge in the same region of Gardner's space of interactions, having followed similar learning paths. A geometric interpretation of Hebbian unlearning is proposed to explain its optimal performances.

I. INTRODUCTION

Hopfield-like neural networks [1] are one of the most studied models for associative memory [2]. In this framework, the network is composed of N binary neurons $\{\sigma_i\}_{i=1}^N = \pm 1$, and it is used to memorize $P = \alpha N$ binary patterns $\{\xi_i^\mu\}_{\mu=1}^P = \pm 1$. By *memorize* we mean that the network must be able to reconstruct the memories on the basis of their noise-corrupted version. This is achieved by endowing it with an appropriate dynamics, such that fixed point attractors with finite basins of attractions are present in close proximity to the memories. If the network is initialized close enough to one of the stored patterns, the dynamics will drive it to the corresponding attractor, reducing the number of misaligned spins. In general, the dynamics is given by a zero temperature asynchronous Monte Carlo dynamics [2, 3], in an energy landscape given by the Hamiltonian

$$H[\sigma] = -\frac{1}{2} \sum_{i,j} J_{ij} \sigma_i \sigma_j. \quad (1)$$

At every step we pick randomly a site i and update the spin according to

$$\sigma_i \rightarrow \text{sign} \left(\sum_{j(\neq i)} J_{ij} \sigma_j \right). \quad (2)$$

The details of the dynamics depend on how the synaptic interaction matrix J is shaped. One of the most influential models in the field is that introduced by Hopfield [1], where the coupling matrix is built according to Hebb's prescription [2, 4]:

$$J_{ij} = \frac{1}{N} \sum_{\mu=1}^P \xi_i^\mu \xi_j^\mu, \quad J_{ii} = 0. \quad (3)$$

The phase diagram of the model has been extensively studied, and includes a recognition phase for $\alpha < \alpha_c \sim 0.14$, where a fraction of the fixed point attractors of the dynamics are very close to the memories ξ^μ [5]. Proximity between two configurations $\bar{\sigma}^1$ and $\bar{\sigma}^2$ is naturally measured in terms of their overlap

$$m = \frac{1}{N} \sum_{i=1}^N \sigma_i^1 \sigma_i^2. \quad (4)$$

In the Hopfield model the overlap between attractors and memories is smaller than 1 for any extensive load $\alpha \neq 0$, and deteriorates as the memory load is increased, up to a discontinuous transition to zero when α_c is reached, which is often referred to as *blackout catastrophe* [2, 6]. Hence, the error correcting performance of a Hopfield network can never be perfect, and the memories are not themselves fixed point of the dynamics.

Many strategies have been proposed in order to extend the capacity of Hopfield-like models, and improve error correcting performance in the retrieval phase [6–12]. In this note we highlight some surprising similarities between two popular options: the *supervised* symmetric perceptron algorithm (SP) [13–15] and the *unsupervised* Hebbian unlearning (HU) algorithm [10, 16–18]. The paper is organized as follows. In Sec. II we introduce the algorithms. In Sec. III and IV we present our main results, and in Sec. V we propose a key to interpret those results. Finally in Sec. VI we summarize our findings.

II. THE ALGORITHMS

In this section we detail how the symmetric perceptron and Hebbian unlearning algorithms operate, and how they improve the performance of the Hopfield model.

* These two authors contributed equally

† Corresponding authors: enzo.marinari@uniroma1.it, giancarlo.ruocco@uniroma1.it, francesco.zamponi@ens.fr

A. The symmetric perceptron

Introducing N -dimensional vectors $(\vec{J}_i)_j := J_{ij}$ and $(\xi^\mu)_i := \xi_i^\mu$, the symmetric perceptron is defined by the following procedure for constructing the matrix J [14, 15]:

- Initialize J_{ij} to a symmetric matrix.
- Update J_{ij} until convergence according to

$$J_{ij} \rightarrow J_{ij} + \lambda \sum_{\mu=1}^P (\epsilon_i^\mu + \epsilon_j^\mu) \xi_i^\mu \xi_j^\mu, \quad J_{ii} = 0, \quad (5)$$

$$\epsilon_i^\mu = \theta(-\Delta_i^\mu + k), \quad \text{where } \Delta_i^\mu = \xi_i^\mu \sum_j \frac{J_{ij}}{|\vec{J}_i|} \xi_j^\mu.$$

Notice that symmetry in the coupling matrix is preserved by the algorithm. The quantities Δ_i^μ are called *stabilities* [19]. The *masks* ϵ_i^μ are defined in such a way that the algorithm stops when $\Delta_i^\mu > k$ for all μ and i , where the stability threshold k is a parameter of the algorithm. If k exceeds a critical threshold $k_{max}(\alpha)$, no symmetric matrix J exists satisfying the stability requirement $\Delta_i^\mu > k$, and the algorithm does not converge (unsatisfiable, or UNSAT, phase). On the other hand, when $k < k_{max}(\alpha)$ such coupling matrices exist, and the algorithm will converge to one of them in a finite number of steps (satisfiable, or SAT, phase). In the limit case $k = k_{max}(\alpha)$, only one coupling matrix meets the stability requirements, and the algorithm is supposed to converge to it, independently on the value of the learning rate λ and of the initial J . It has been shown that, as one could expect, increasing k towards k_{max} leads not only to more stable memories, but also to larger basins of attraction for each memory [15].

An elegant way to understand the role of k is recasting the stability problem in terms of a linear regression [20]: for every pattern and every spin, we define N -dimensional *patterns*

$$\vec{\eta}_i^\mu = \xi_i^\mu \vec{\xi}^\mu. \quad (6)$$

Now the stabilities can be expressed as the scalar product

$$\Delta_i^\mu = \frac{\vec{J}_i \cdot \vec{\eta}_i^\mu}{|\vec{J}_i|}, \quad (7)$$

and the constraint $\Delta_i^\mu > k$ is satisfied when vector $\vec{\eta}_i^\mu$ lies on the positive side of the oriented plane normal to \vec{J}_i and passing through the origin, at a distance greater than k from it. In these terms, the problem of perfectly stabilizing a number P of N -dimensional patterns has been factorized into N independent linear separation problems, each classifying a number P of N -dimensional vectors. The symmetric perceptron algorithm solves this separation problem under the condition $J_{ij} = J_{ji}$.

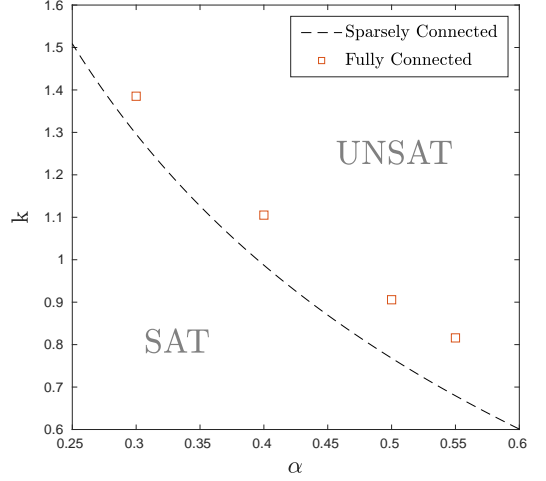


FIG. 1. Phase diagram of the linear symmetric perceptron. The dashed line is for the analytical results for $k_{max}(\alpha)$ obtained by ref. [14] for slightly diluted networks. Squares show numerical results for $k_{max}(\alpha)$ in a fully connected model at $\alpha \in \{0.3, 0.4, 0.5, 0.55\}$. Simulations have been run at different sizes of the network to measure the probability for the algorithm to converge before 10^3 steps of the training (hence providing a lower bound to the actual value of stability). A finite size scaling analysis has been used to extrapolate the value of $k_{max}(\alpha)$ to the thermodynamic limit.

The function $k_{max}(\alpha)$ has been determined analytically [14] for slightly diluted recurrent networks, i.e. networks with an average connectivity scaling as $\log N$. Numerical results from the study of the algorithm defined in eq. (5) on networks that are both fully connected and fully symmetric suggest that, for the same degree of symmetry, k_{max} at a given α is located slightly above the one predicted by [14]. This finding, discussed in Fig. 1, suggests to reconsider previous interesting analyses [21] and opens the road to further investigations of the critical capacity as a function of the network connectivity [22].

Since we are analyzing the close relationship between the symmetric perceptron and Hebbian unlearning (see Sec. II B), we always initialize the couplings according to Hebb's rule, Eq. (3), keeping in mind that results for $k = k_{max}(\alpha)$ should not depend on this choice. In Fig. 2 we plot the evolution with the number of steps t of $\Delta_{min} := \min_{i,\mu} \{\Delta_i^\mu\}$, $\Delta_{max} := \max_{i,\mu} \{\Delta_i^\mu\}$ and $\Delta_{av} := 1/(PN) \sum_{i,\mu} \Delta_i^\mu$, each averaged over many random realizations of the memories $\vec{\xi}$. One sees that the SP algorithm, while slightly reducing Δ_{av} and Δ_{max} , increases the value of Δ_{min} from negative values (i.e. not all memories are stable) to positive values (i.e. all memories are stable) and up to the prescribed threshold k . The same profile of the stabilities is obtained at different choices of the control parameters, when $k \leq k_{max}(\alpha)$.

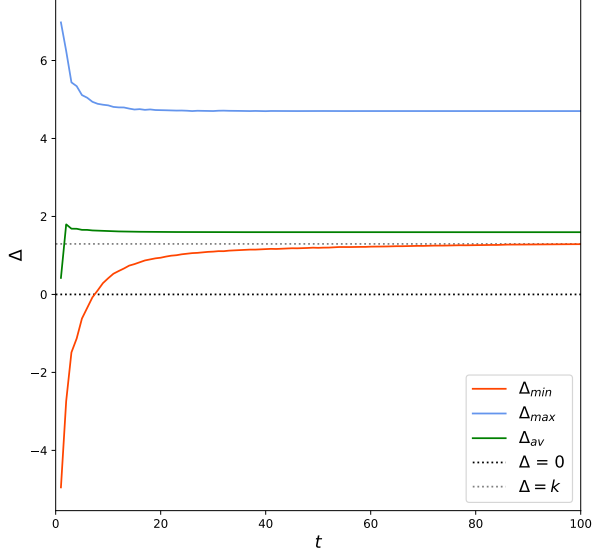


FIG. 2. As an example, the values of Δ_{min} , Δ_{max} and Δ_{av} are plotted as a function of the number of iterations t of the SP, averaged over 50 realizations of the memories, at $N = 800$, $\alpha = 0.3$, $\lambda = 1$.

B. Hebbian unlearning

A very interesting proposal to increase the performance of the Hopfield model consists of modifying the Hebbian learning rule defined in eq. (3) by adding to it a “dreaming” procedure [10, 11]. This goes as follows: initialize the coupling matrix according to Eq. (3), and then repeat D times the following steps:

- Initialize the neurons to a random state, and follow the dynamics until it converges to a fixed point $\vec{\sigma}^*$.
- Modify the coupling matrix according to

$$J_{ij} \rightarrow J_{ij} - \frac{\epsilon}{N} \sigma_i^* \sigma_j^* . \quad (8)$$

It is easy to see that at each step the energy of the configuration $\vec{\sigma}^*$ reached by the algorithm is increased, making it less stable. Since every memory is surrounded by many spurious local energy minima, which intercept virtually every dream, the overall effect is a smoothing of the energy landscape around the attractors correlated to the memories, by destabilizing other attractors. This procedure is often referred to as Hebbian unlearning. The total number of dreams D is a parameter of the algorithm, and must be chosen as to maximize the recognition performance at a given load α . It has been shown that this procedure improves the performance of the model in two ways [16–18, 23]: on the one hand, the critical memory load is increased up to $\alpha_c^{HU} \sim 0.6$. On the other hand,

the overlap between the attractors and the memories goes to one, meaning that memories become real fixed points of the dynamics.

This last fact, which is especially remarkable because the dreaming procedure is unsupervised, led us to try and characterize the performance of the algorithm in terms of the stabilities Δ_i^μ introduced in Sec. II A. This approach has already been attempted [24], and our analysis pushes it further and reveals new unexpected features. In fig. 3 we show the typical behavior of Δ_{min} , Δ_{av} and Δ_{max} as the unlearning procedure unfolds. The horizontal axis represents the number of steps D performed by the algorithm, rescaled by ϵ/N . The reason for this choice will become clear later. Focusing on Δ_{min} , we can see a non-monotonic behavior: the minimal stability grows to positive values, peaks at some value $D = D_{top}$ and then decreases back to negative values. Between D_{in} and D_{fin} every stability is positive or, equivalently, every memory is a fixed point for the dynamics. As we increase α , the interval $[D_{in}, D_{fin}]$ shrinks, and the height of the peak at D_{top} lowers, until we reach a critical load α_c , above which Δ_{min} never goes above zero. Collecting data for networks of size $N = 300, 400, 500, 600, 800$ it is possible to extrapolate the position of D_{in} , D_{top} and D_{fin} as a function of α , ϵ and N , as well as the critical capacity α_c . We found that the number of dreams is in every case proportional to N/ϵ , and that the rescaled variable $D_{top}\epsilon/N$ depends linearly on α , up to the critical value

$$\alpha_c^{HU} = 0.589 \pm 0.003 ,$$

above which it is not defined anymore. These results are consistent with those presented in [17]. We also found that the dependence on α of $(D_{top} - D_{in})\epsilon/N$ and $(D_{fin} - D_{top})\epsilon/N$ is well described by a power law with exponent $1/2$, in proximity of α_c . The resulting scaling relations are:

$$D_{top}(\epsilon, \alpha, N) = \frac{N}{\epsilon} (a \cdot \alpha + b) , \quad (9)$$

$$D_{in}(\epsilon, \alpha, N) = D_{top} - \frac{N}{\epsilon} (c \cdot \alpha + d)^{1/2} , \quad (10)$$

$$D_{fin}(\epsilon, \alpha, N) = D_{top} + \frac{N}{\epsilon} (e \cdot \alpha + f)^{1/2} , \quad (11)$$

with

$$a = 1.02 \pm 0.02 , \quad b = -0.05 \pm 0.01 ,$$

$$c = -0.039 \pm 0.003 , \quad d = 0.023 \pm 0.002 ,$$

$$e = -0.022 \pm 0.001 , \quad f = 0.013 \pm 0.001 .$$

All the statistical errors have been evaluated using the jackknife method.

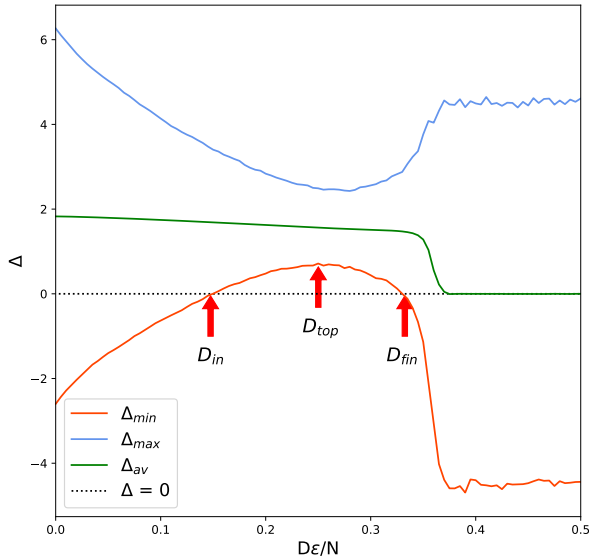


FIG. 3. Values of Δ_{min} , Δ_{max} and Δ_{av} computed during Hebbian unlearning, averaged over 50 realizations of the memories at $N = 800$, $\alpha = 0.3$, $\epsilon = 10^{-2}$. Data for D_{in} , D_{top} and D_{fin} are denoted by the red arrows.

III. BASINS OF ATTRACTION

We have also compared the performance of SP and HU by measuring the shape of the basins of attraction around each memory. This is done by initializing the network at some fixed distance m_i from one of the memories ξ_i^μ and following the dynamics until convergence to a fixed point $\bar{\sigma}^*$ is reached. Then, we measure the overlap between $\bar{\sigma}^*$ and ξ_i^μ , averaged over many realizations of the memories:

$$m_f = \frac{1}{N} \sum_i^N \langle \xi_i^\mu \sigma_i^* \rangle. \quad (12)$$

In Fig. 4 we plot m_f as a function of m_i . Colored dashed curves refer to SP for different values of k , up to the highest k that allows the algorithm to converge in $O(10^3)$ iterations. This slight underestimations of the real $k_{max}(\alpha)$ bares very little consequences to our results. Related to this, we underline the importance of the choice of λ at a given value of N . This is another crucial topic that is rarely discussed in the literature. Higher values of λ imply larger learning steps, while smaller values are associated to a finer exploration of space of coupling matrices during training. It is observed that the algorithm, operating at $\lambda = 1, 10^{-1}, 10^{-2}$, converges to almost identical matrices already when k is equal to the maximal stability for diluted networks [14] that, according to Fig. 1, is slightly lower than the actual k_{max} . This suggests that the final state lies very closely to the unique optimal so-

lution even when we are not exactly at k_{max} . Hence, no significant changes are expected in our numerical results when k is pushed further towards its maximal value. On the other hand, when λ assumes smaller values, i.e. $\lambda = 10^{-3}, 10^{-4}, 10^{-5}$, basins are observed to be smaller in size and the volume of solutions is larger, indicating that the final state remains farer from the maximal performance. In order to recover the numerical results obtained at a larger λ , one needs to progressively increase k to values that are difficult to reach numerically. As a result, the choice of $\lambda = 1$ in this section seems to us well justified to reproduce the optimal performance of the symmetric perceptron at $k \sim k_{max}$.

Consistently with the literature, we find that increasing the stability leads to an increase of m_f at fixed m_i [15]. In particular, when the stability is equal to zero, the memories, albeit being fixed point of the dynamics, have zero basin of attraction, as indicated by the very low values of m_f for $m_i \neq 1$. The gray dashed line at the bottom of Fig. 4 refers to the Hopfield model without dreaming: since $\alpha > 0.14$ the model does not learn. The colored continuous lines refer to Hebbian unlearning, for different amounts of dreaming. More specifically, we measured the performance of the model for the three values $D = D_{in}$, D_{top} , and D_{fin} defined in Sec. II B. It is clear how dreaming improves the performance of the network, and we found that the performance is not maximized at $D = D_{top}$ as one could expect [24], but at $D = D_{in}$, where the requirement for perfect retrieval of the memories is satisfied with zero margin.

We also found that the performance of Hebbian unlearning at $D = D_{in}$ and the one of the SP at $k \simeq k_{max}$ are indistinguishable within our numerical resolution. This is a remarkable fact, since the two algorithms have a radically different structure: the SP algorithm is supervised, i.e. it needs to have access at every step to all the memories that the network needs to memorize, while the HU is not, and only exploits the topology of the spurious states generated by Hebb's prescription in Eq. (3). These findings are robust to change in the load α and to finite size effects, as illustrated in Fig. 5. The mean basin radius at finite N is defined as $1 - m_i$, selecting the value of m_i below which more than 30% of the patterns are reconstructed with more than 5% error. The dots represent our extrapolation of this quantity to the limit $N \rightarrow \infty$, for different values of α . The lower dots relative to the SP correspond to $k < k_{max}$, and the value of the mean basin radius gets higher as k is increased up to $k \simeq k_{max}$. Again, one can see that even in the thermodynamic limit, our simulations suggest that in their optimal regime the two algorithms perform essentially in the same way.

IV. SPACE OF INTERACTIONS

One way to visualize the solutions of the optimization problem, and the way these solutions are reached by

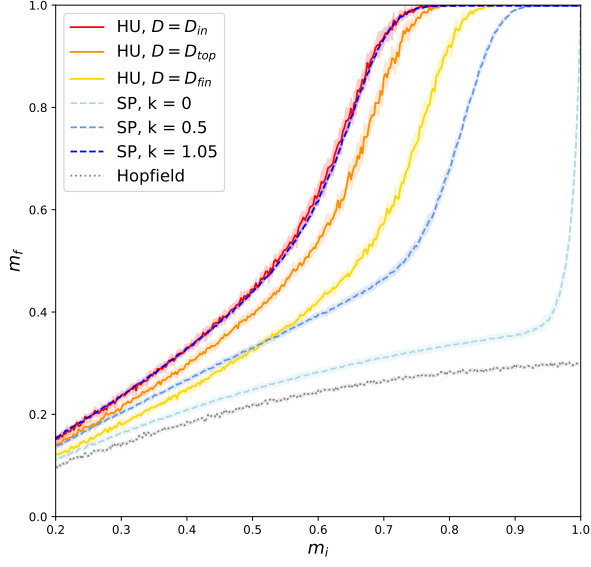


FIG. 4. The average size of basins of attraction at $N = 800$, $\alpha = 0.4$ for both SP and HU, averaged over several realizations of the disorder. Continuous lines are for basins at D_{in} , D_{top} and D_{fin} for HU with $\epsilon = 10^{-2}$. Dashed lines are for three values of k , including the $k \sim k_{max}$, used for SP with $\lambda = 1$. The gray dotted line represents the performance of the Hopfield model at the same value of α . The filled area represents the statistical errors.

means of the algorithm, is to exploit the space of interactions as conceived by Gardner [13]. Consider a spherical surface in $N(N-1)/2 - 1$ dimensions where each point is a vector composed by the off-diagonal elements $J_{j>i}$ of the connectivity matrix normalized by their standard deviation. These position vectors hence will be

$$\vec{r} = \vec{J}/\sigma_J, \quad (13)$$

with

$$\sigma_J = \sqrt{\frac{2}{N(N-1)} \sum_{i<j}^{1,N} J_{ij}^2}. \quad (14)$$

For what concerns the SP, after fixing the value of α and a set of patterns, one can imagine the sphere as composed by an UNSAT and a SAT region. These regions are connected sub-spaces of the original sphere, so that one can go from a matrix to another one in a continuous fashion. The SAT region contains the point relative to the unique solution at $k = k_{max}(\alpha)$.

We now define an *overlap* parameter quantifying the covariance of two generic symmetric matrices J_{ij} and U_{ij}

$$q = \frac{2}{N(N-1)} \sum_{i<j}^{1,N} \langle \frac{J_{ij}U_{ij}}{\sigma_J\sigma_U} \rangle, \quad (15)$$

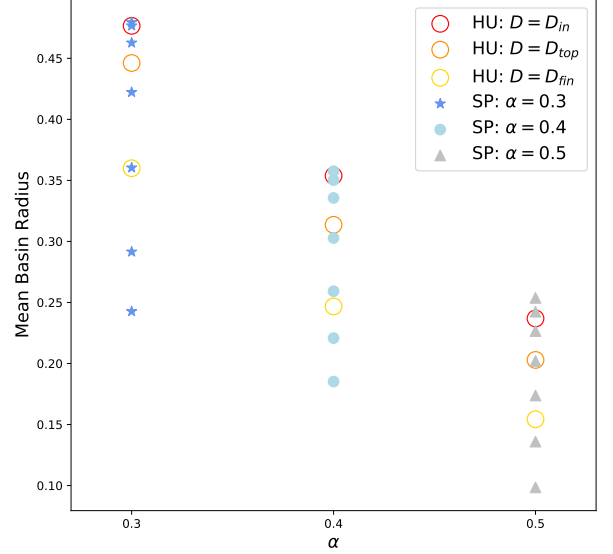


FIG. 5. Asymptotic values of the mean radius of the basins of attraction for both SP and HU, measured as in [15] for $\alpha = 0.3, 0.4, 0.5$ and $\lambda = 1$. Points for the SP correspond to the following values of k : $\alpha = 0.3$, $k \in \{0.4, 0.5, 0.7, 0.9, 1.1, 1.296, 1.32\}$; $\alpha = 0.4$, $k \in \{0.4, 0.5, 0.6, 0.75, 0.9, 0.988, 1.05\}$; $\alpha = 0.5$, $k \in \{0.3, 0.4, 0.5, 0.6, 0.7, 0.768, 0.85\}$. Error bars are smaller than the symbols size.

where $\langle \cdot \rangle$ is the average over the disorder.

A. Final States

We first evaluate the final points where the two algorithms converge in the space of interactions. Hebbian Unlearning is stopped at $D = D_{in}$ as that is the relevant amount of *dreams* identified in Sec. II B. The Symmetric Perceptron is run at $\lambda = 1$. Fig. 6(left) displays the overlap between the resulting matrices when the SP is performed at different values of k before reaching $k_{max}(\alpha)$. The plot shows that q increases with k , suggesting that HU pushes the system to the same region of solutions where the SP converges when k is close to k_{max} . Finite size effects evidently appear near the abrupt transition from SAT to UNSAT, but the increase of q with the size of the network suggests that the maximum overlap might be associated to the maximal stabilities when N becomes large enough.

The plot of q as a function of α , see Fig. 6(right), shows how the distance between the final points and the initial Hebbian matrix increases when the number of memories becomes larger, while the distance between the two final points remains small and stable for $\alpha < \alpha_c^{HU}$.

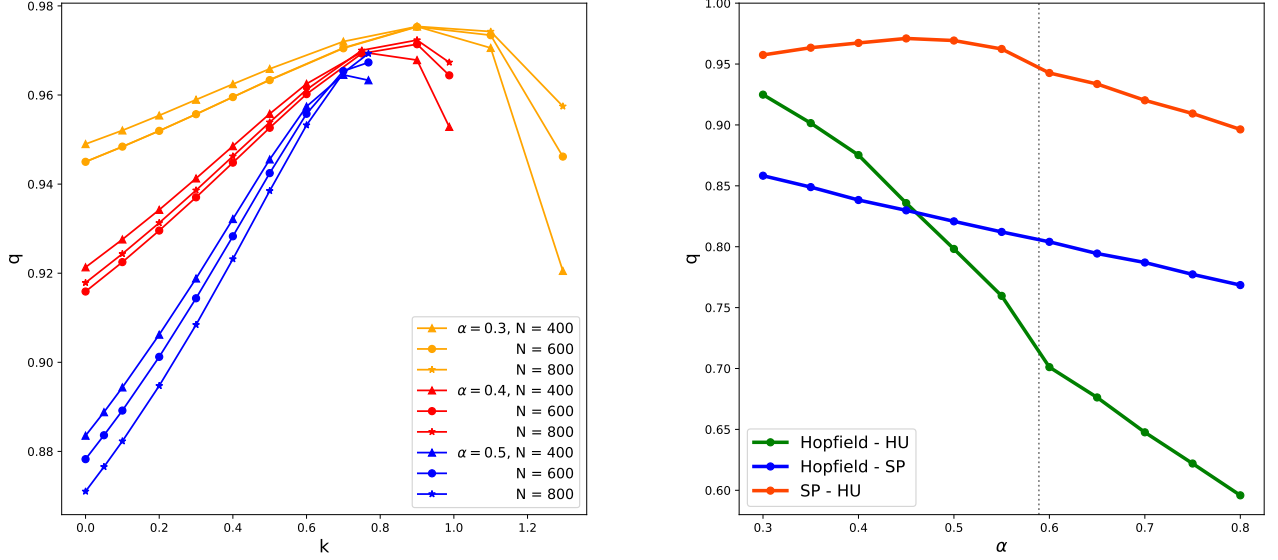


FIG. 6. Left: Overlap q between the final states of HU with $\epsilon = 10^{-2}$ at $D = D_{in}$ and SP with $\lambda = 1$ having reached a stability k . Measures are for different values of N and α and points represent the mean computed over 5 realizations of the disorder. Error bars are smaller than the data symbol. Values of k range from 0 to slightly below $k_{max}(\alpha)$. Right: Overlap q as a function of α at $N = 800$. Points represent the mean of 10 realizations of the disorder and error bars are smaller than the data symbol. The orange symbols correspond to the overlap between the final states of HU with $\epsilon = 10^{-2}$ at $D = D_{in}$ and SP with $\lambda = 1$ and k close to $k_{max}(\alpha)$. The overlap between the initial Hebbian matrix and the final state of the HU (green) or SP (blue) with the same choice of the parameters is also shown. The critical capacity for the HU is represented by the gray dotted line.

B. Learning Paths and Gradients

By comparing the final states of convergence as done in Sec. IV A we conclude that two networks, starting from the same initial matrix, end up in very similar configurations of the couplings J_{ij} . Now we analyze the whole trajectory traced by the two algorithms in the space of interactions.

We set $\alpha = 0.55$, so that the overlap between the initial and the final state is small enough, i.e. they are distant on the sphere, $N = 800$, $\lambda = 10^{-4}$ and k close to k_{max} in one single sample. The choice of a small value of the learning rate λ allows to trace a continuous path in the space of the interactions. HU is run choosing $D = D_{in}$ for 10 samples in total. Fig. 7(left) reports the projection of the resulting trajectories in the space of J along three randomly chosen directions. The plot shows that the two algorithms explore the same region of the space of interactions, proceeding along a similar direction. We also observe that the convergence velocities of the two algorithms are very different. Indicating with t the time steps for both processes, Fig. 7(right) shows the logarithm of the absolute value of the *velocity* of the algorithm, defined as

$$\Delta \vec{J}^{(t)} = \vec{J}^{(t+1)} / \sigma_J^{(t+1)} - \vec{J}^{(t)} / \sigma_J^{(t)}. \quad (16)$$

The direction of this vector defines the gradient followed by the algorithm in the space of interactions at a given time step.

While the convergence speed of the HU does not significantly vary, the SP shows, at any scale of λ , an acceleration in time that resembles an exponential law. In other words, while HU explores the space of interactions nearly uniformly in speed, the SP takes about $15 \div 20$ time steps to reach a smaller condensed region where it gets confined until convergence.

The different speeds of the algorithms imply an inherent difficulty in comparing the trajectories *point-by-point*. Our analysis will thus rely on defining a particular direction \hat{v} in the space of interactions that we will use to compare the two trajectories and their gradients. Such a direction is defined by the line that connects the initial Hebbian matrix with the point of convergence of the SP,

$$\hat{v} = \frac{\vec{J}_{SP}^{(t_{max})} / \sigma_{SP}^{(t_{max})} - \vec{J}^{(0)} / \sigma^{(0)}}{|\vec{J}_{SP}^{(t_{max})} / \sigma_{SP}^{(t_{max})} - \vec{J}^{(0)} / \sigma^{(0)}|}. \quad (17)$$

We can now define two time-dependent observables that can help us in the analysis of the trajectories:

$$q_v(t) = \frac{\vec{J}^{(t)} / \sigma^{(t)} - \vec{J}^{(0)} / \sigma^{(0)}}{|\vec{J}^{(t_{max})} / \sigma^{(t_{max})} - \vec{J}^{(0)} / \sigma^{(0)}|} \cdot \hat{v}, \quad (18)$$

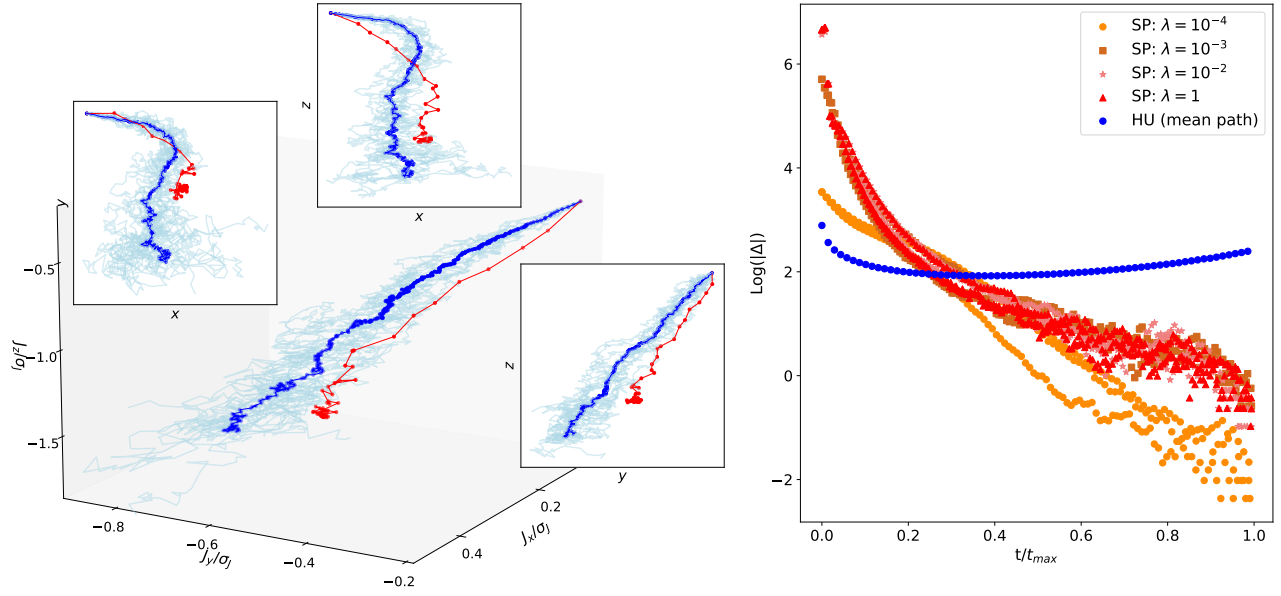


FIG. 7. Left: 3-dimensional projection of the trajectories followed by the system in the space of interactions during the dynamics of HU and SP. Numerical measurements have been taken for one sample at $N = 800$ and $\alpha = 0.55$, $\epsilon = 10^{-2}$, $\lambda = 10^{-4}$. 10 trajectories of the HU are drawn in light blue, while the average unlearning path is in blue. The path followed by the SP is depicted in red. Points represent different steps of the algorithms. HU has been resampled at regular intervals along the trajectory for simplicity of the data analysis. Right: Absolute value of the velocity $\Delta\vec{J}$ in logarithmic scale as a function of the normalized time scale t/t_{max} where t_{max} is the maximum number of steps reached by the algorithm in a given sample. Numerical measurements are for one sample at $N = 800$ and $\alpha = 0.55$, $\epsilon = 10^{-2}$, $\lambda = 1, 10^{-2}, 10^{-4}$. Three samples were simulated for the SP and one sample for the HU.

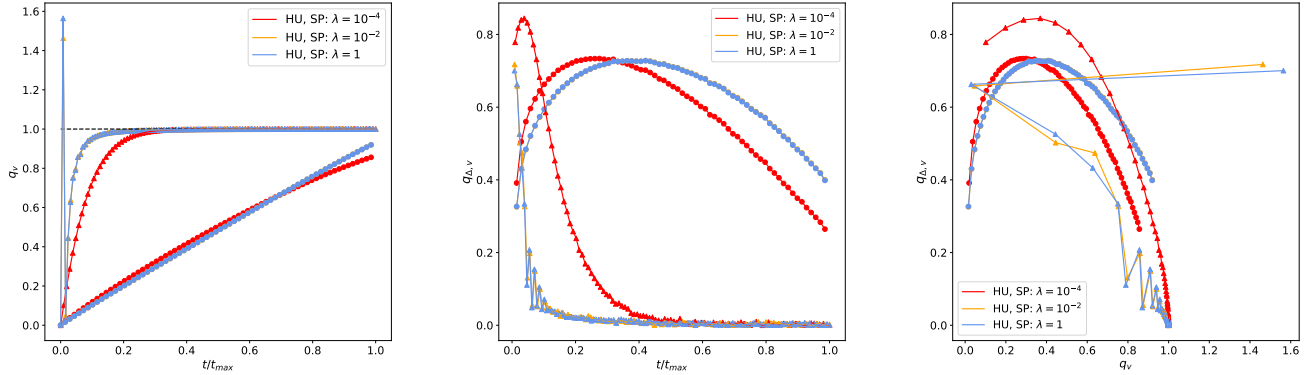


FIG. 8. Left: Effective overlap distance q_v as a function of time. Center: Projection of the velocity along the direction \hat{v} as a function of time. Right: The direction of the velocity $q_{\Delta,v}$ as a function of the distance q_v . Numerical measurements are collected from one single sample at $N = 800$ and $\alpha = 0.55$ at $\epsilon = 10^{-2}$ for the HU (circles) and different values of λ for the SP (triangles).

which is a measure of the angular distance of any point of the trajectory from the line traced by the direction \hat{v} at time t , with $q_v(t) \in [0, 1] \forall t$. The smaller this quantity is, the more evidently the trajectory is diverging from \hat{v} .

One can also introduce

$$q_{\Delta,v}(t) = \frac{\vec{J}^{(t+1)}/\sigma^{(t+1)} - \vec{J}^{(t)}/\sigma^{(t)}}{|\vec{J}^{(t+1)}/\sigma^{(t+1)} - \vec{J}^{(t)}/\sigma^{(t)}|} \cdot \hat{v}, \quad (19)$$

that is, the projection of the velocity of the algorithm at

the step t along the direction \hat{v} . The larger this quantity is, the more aligned to \hat{v} the trajectory is.

Fig. 8(left) represents the values of q_v during the same trajectory that is depicted in fig. 7(left). One can see that $q_v(0)$ is small for both the HU and the SP. This means that they both start in the wrong direction: this is particularly reasonable for the HU, which involves a random picking of the initialization state. However, while the SP rapidly reaches $q_v = 0$ because of its high initial acceleration at all the considered values of λ , in the HU algorithm q_v is decreasing at lower rate. An initial overshooting of the SP at high values of λ is signaled by an anomalously high value of q_v at the second step of the process.

The directions followed by the two algorithms with respect to \hat{v} are shown in Fig. 8(center). The SP at $\lambda = 10^{-4}$ has a peak in $q_{\Delta,v}$ in the first part of the trajectory, signaling a high degree of alignment between the gradient and \hat{v} . Later on, the SP rapidly converges towards the condensed region, where gradients lose their polarization with \hat{v} , but the convergence point has already been reached. When higher values of λ are used, no relevant polarization is measured. The HU shows a similar behavior: the trajectory starts along a direction that is barely aligned with \hat{v} but a consistently high degree of alignment is obtained after more or less half of the iterations. Eventually, the HU also converges towards the final state losing the alignment with \hat{v} . Fig. 8(right) displays the direction of the velocity as a function of the distance from \hat{v} .

Summing up, three phases of the trajectory can be roughly recognized for both algorithms: one first phase in which the system moves away from \hat{v} after a bad start; a second phase of alignment; a third phase in which the matrix plunges towards the convergence state.

V. GEOMETRIC INTERPRETATION OF UNLEARNING

In order to provide an argument that might explain the similarities between the HU and SP algorithms, we rewrite the rule in Eq. (8) in a vectorial fashion,

$$\vec{J}_i^{(D+1)} = \vec{J}_i^{(D)} - \frac{\epsilon}{N} \vec{\eta}_i^*, \quad (20)$$

where \vec{J}_i is the vector of the elements contained in the i^{th} row of the connectivity matrix and we call $\vec{\eta}_i^*$ a *glassy pattern*, defined in analogy with the memory patterns $\vec{\eta}_i^\mu$ as follows

$$\vec{\eta}_i^* = \sigma_i^* \vec{\sigma}^*. \quad (21)$$

We also introduce the perceptron overlap

$$\omega_i^\mu = \left\langle \frac{1}{N} \vec{\eta}_i^* \cdot \vec{\eta}_i^\mu \right\rangle, \quad (22)$$

where the overbar indicates an average over the glassy states in a given realization of the disorder. Each pair

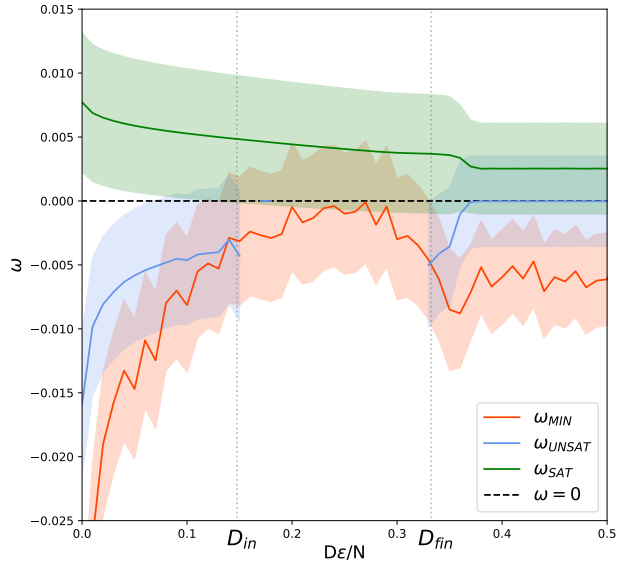


FIG. 9. Mean values assumed by the perceptron overlap ω for SAT, UNSAT and *min* patterns during the HU process. Measurements are performed at $N = 800$, $\alpha = 0.3$, $\epsilon = 10^{-2}$ over 200 glassy states and several realizations of the disorder. Error bars are indicated by the shaded region.

(i, μ) is thus related to a given constraint of the associated optimization problem, with $\Delta_i^\mu \geq 0$ for SAT constraints, and $\Delta_i^\mu < 0$ for UNSAT ones. Fig. 9 shows ω_i^μ at $\alpha = 0.3$ and $N = 800$ for the three types of constraints: SAT, UNSAT and *minimally satisfied*, i.e. the SAT constraints with the lowest measured stability. The fact that the perceptron overlap is negative for both UNSAT and *min* constraints, but positive for SAT constraints, suggests that the distribution of the $\vec{\eta}_i^\mu$ looks anisotropic from the reference frame of the glassy patterns. This is certainly induced by the fact that glassy patterns $\vec{\eta}_i^*$ are SAT by definition, so they are more likely to be contained in the same half of hyperspace, defined by the orthogonal plane to \vec{J}_i , that contains SAT memory patterns.

Moreover, since there is a minus sign on r.h.s. of Eq. (20), HU is performing the same geometric transformation of the perceptron in order to align the \vec{J}_i vectors to the memory patterns $\vec{\eta}_i^\mu$. By only exploiting the landscape of the glassy states of the Hopfield model out of the retrieval regime, the HU algorithm manages to accomplish this task in an optimal way. We suppose that the small, but yet non null, overlap of glassy states with the memories is an important feature to ensure the maximization of the size of the basins of attraction.

VI. CONCLUSIONS

We have analyzed two algorithms that are able to restore the classification properties of the Hopfield model in the non-retrieval regime. Hebbian unlearning is unsupervised and it only relies on the distribution of the spurious minima of the Hamiltonian. On the other hand, the symmetric perceptron is based on a supervised procedure.

We have found that the best number of iterations of the HU procedure is $D = D_{in}$, given by Eq. (10), at variance with [24], where the optimal state of the network was assumed to coincide with the highest minimum stability, in analogy with [19]. We have measured the average size of the basins of attraction. HU performs consistently with the SP near the maximal stability k . This result suggests the HU to be an optimal unsupervised algorithm in terms of generalization of the network: from a Hebbian perspective large basins of attraction imply the capability of the model to associate more exotic stimuli to known memories, i.e. a higher recognition power with respect to new inputs. According to Fig. 4 a SP at $k = 0$ has no generalization capabilities, meaning that it falls into an overfitted regime, where memories are recognized only if the initial state of the dynamics coincides with the memory itself. An increasing value of k is related to an increase in generalization. HU is able to reach the highest degree of generalization in a spontaneous and unsupervised fashion.

We have studied the trajectories of the matrix J in the space of interactions. The final states of the algorithms maximize the overlap between matrices, suggesting that the algorithms converge to the same regions of the interaction space. In the middle part of the trajectory the two algorithms also explore nearby regions, suggesting that they both follow well overlapping gradients in the space of the couplings.

By empirically measuring the overlap between memory patterns and glassy patterns we have established that the HU rule in Eq. (8) represents a valid, yet counterintuitive, transformation that mimics the linear regression operation performed by a perceptron while conserving a local effect on the couplings.

A very close analogy between the effects of these two formally different rules has emerged. Our results shed light on a substantial mechanism that might help to understand real neuro-physiological processes lying behind synaptic development in the brain [25] and dream-sleep in mammals [26]. In the context of dream-sleep, it is important to remind that Hebbian unlearning has been introduced simultaneously with another remarkable contribution by Crick and Mitchinson [27]. Their paper conjectured a sort of *reverse learning* procedure which assigned, for the first time, a biological function to dreams, over-

coming their description as mere epiphenomena of neural activity. Such a procedure strongly resembles Hopfield's unlearning. Kinouchi and Kinouchi [28] provided some biological examples that might encourage to investigate this type of synaptic transformation, even though a clear evidence of its existence has not been shown yet. Furthermore, a recently published review by Hoel [29] corroborates the evolutionary significance of dreams in terms of the generalization performances of neural networks. Dreams, due to their hallucinoid contents, are responsible for noise injection in the learning procedure, in analogy with dropout [30] techniques used in machine learning: a dreaming neural network is thus able to generalize better, avoiding over-fitting. The importance of noise addition in learning is also suggested by other recent studies that try to increase generalization in deep neural networks by taking inspiration from biology [31, 32]. According to these works, a local Hebbian-like action on synapses can ensure decorrelation of the stored patterns, and thus avoid confusion. We do believe that what we found in the Hopfield model is coherent with such a picture: Hebbian Unlearning is not a form of *reverse* learning, as repetitively stated in the past literature, but it is rather responsible of the learning of noisy versions of the memories, which help to minimize over-fitting.

One possible development of this research might deal with memories presenting strong structural correlations such as images. In this case a linear regression operation, as the one performed by linear perceptrons, may not be sufficient to ensure classification. It has been shown that Hebbian unlearning works well even with digits [17]. We suggest that such correlations, being encoded in the quenched disorder of the system, and thus in the glassy landscape of attractors, might drift the learning path right to the optimal region of the space of interactions. Another direction for future work would be the verification of the results on other types of models, such as more biologically reliable Hopfield-like networks [33], random neural networks [34, 35], or continuous attractor neural networks [36]. This last class of systems, which aim at describing the functioning of the spatial memory encoded in the hippocampal synapses, might open the way to experiments and inferential analyses of real data, allowing a proper research of physiologic unlearning-like mechanisms in the brain.

Finally, these ideas could possibly find application and analogies in the training of physical systems, such as meta-materials or allosteric networks, see e.g. [37, 38].

ACKNOWLEDGMENTS

We thank Dario Lippi for his important contribution during the first stage of this work.

[1] J. Hopfield, Neural networks and physical systems with emergent collective computational abilities, Proc. NatL

Acad. Sci. USA **79**, 2554 (1982).

- [2] D. J. Amit, *Modeling Brain Functions: The world of Attractor Neural Networks* (Cambridge University Press, 1989).
- [3] P. Peretto, Collective properties of neural networks: A statistical physics approach, *Biol. Cybern.* **50**, 51 (1984).
- [4] D. O. Hebb, *The organization of behavior: a neuropsychological theory* (Wiley, 1949).
- [5] D. Amit, H. Gutfreund, and H. Sompolinsky, Storing infinite numbers of patterns in a spin-glass model of neural networks, *J. Stat. Phys.* **15**, 1530 (1985).
- [6] M. Benedetti, V. Dotsenko, G. Fischetti, E. Marinari, and G. Oshanin, Recognition capabilities of a hopfield model with auxiliary hidden neurons, *Phys. Rev. E* **103**, L060401 (2021).
- [7] I. Kanter and H. Sompolinsky, Associative recall of memory without errors, *Phys. Rev. A* **37**(1), 380 (1987).
- [8] V. Dotsenko, N. Yarunin, and E. Dorotheyev, Statistical mechanics of hopfield-like neural networks with modified interactions, *J. Stat. Phys.* **24**, 2419 (1991).
- [9] A. Plakhov and S. Semenov, The modified unlearning procedure for enhancing storage capacity in hopfield network, *RNNS/IEEE Symposium on Neuroinformatics and Neurocomputers* (1992).
- [10] J. Hopfield, D. Feinstein, and R. Palmer, Unlearning has a stabilizing effect in collective memories, *Nature* **304**, 158 (1983).
- [11] A. Fachechi, E. Agliari, and A. Barra, Dreaming neural networks: forgetting spurious memories and reinforcing pure ones, *Neural networks* **112**, 24 (2019).
- [12] V. Folli, M. Leonetti, and G. Ruocco, On the maximum storage capacity of the hopfield model, *Front. Comput. Neurosci.* **10**, 144 (2017).
- [13] E. Gardner, The space of interactions in neural network models, *J. Phys. A* **21**, 257 (1988).
- [14] E. Gardner, H. Gutfreund, and I. Yekutieli, The phase space of interactions in neural networks with definite symmetry, *J. Phys. A* **22**, 1995 (1989).
- [15] B. Forrest, Content-addressability and learning in neural networks, *J. Phys. A* **21**, 245 (1988).
- [16] J. L. van Hemmen, L. Ioffe, R. Kühn, and M. Vaas, Increasing the efficiency of a neural network through unlearning, *Physica A* **163**, 386 (1990).
- [17] J. L. van Hemmen and N. Klemmer, *Unlearning and Its Relevance to REM Sleep: Decorrelating Correlated Data*, edited by J. Taylor, E. Caianiello, R. Cotterill, and J. Clark (Springer, London, UK, 1992).
- [18] S. Wimbauer, N. Klemmer, and J. L. van Hemmen, Universality of unlearning, *Neural Networks* **7**, 261 (1994).
- [19] W. Krauth, J.-P. Nadal, and M. Mezard, The roles of stability and symmetry in the dynamics of neural networks, *J. Phys. A* **21**(13), 2995 (1988).
- [20] M. Minsky and S. Papert, *Perceptrons: an introduction to computational geometry* (MIT Press, 1969).
- [21] A. Theumann, Space of interactions with definite symmetry in neural networks with biased patterns as a spin-glass problem, *Phys. Rev. E* **53**(6), 6361 (1996).
- [22] F. Aguirre-Lopez, M. Pastore, and S. Franz, in preparation (2022).
- [23] D. Kleinfeld and D. Pendergraft, Unlearning increases the storage capacity of content addressable memories, *Biophys. J.* **51**, 47 (1987).
- [24] J. Horas and P. Pasinetti, On the unlearning procedure yielding a high-performance associative memory neural network, *J. Phys. A* **31**, L463 (1998).
- [25] U. Farooq and G. Dragoi, Emergence of preconfigured and plastic time-compressed sequences in early postnatal development, *Science* **363**, 168 (2019).
- [26] J. Payne and L. Nadel, Sleep, dreams, and memory consolidation: The role of the stress hormone cortisol, *Learn Mem.* **11**(6), 671 (2019).
- [27] F. Crick and G. Mitchison, The function of dream sleep, *Nature* **304**, 111 (1983).
- [28] O. Kinouchi and R. Kinouchi, Dreams, endocannabinoids and itinerant dynamics in neural networks: re-laborating the crick-mitchison unlearning hypothesis, *arXiv:cond-mat/0208590* (2002).
- [29] E. Hoel, The overfitted brain: Dreams evolved to assist generalization, *Patterns* **2**(5), 100244 (2021).
- [30] N. Srivastava, G. Hinton, A. Krizhevsky, I. Sutskever, and R. Salakhutdinov, Dropout: A simple way to prevent neural networks from overfitting, *Journal of Machine Learning Research* **15**, 1929 (2014).
- [31] T. Tadros, G. Krishnan, R. Ramyaa, and B. M., Biologically inspired sleep algorithm for increased generalization and adversarial robustness in deep neural networks, *International Conference on Learning Representations* (2019).
- [32] J. Dapello, J. Feather, H. Le, T. Marques, D. Cox, J. McDermott, J. DiCarlo, and S. Chung, Neural population geometry reveals the role of stochasticity in robust perception, *NeurIPS Proc.* (2021).
- [33] A. Treves and D. J. Amit, Metastable states in asymmetrically diluted hopfield networks, *J. Phys. A* **21**, 3155 (1988).
- [34] S. Hwang, V. Folli, E. Lanza, G. Parisi, G. Ruocco, and F. Zamponi, On the number of limit cycles in asymmetric neural networks, *J. Stat. Mech: Theory and Experiments* **5**, 053402 (2019).
- [35] S. Hwang, V. Folli, E. Lanza, G. Parisi, J. Rocchi, G. Ruocco, and F. Zamponi, On the number of limit cycles in diluted neural networks, *J. Stat. Phys.* **181**(6), 2304 (2020).
- [36] A. Battista and R. Monasson, Capacity-resolution trade-off in the optimal learning of multiple low-dimensional manifolds by attractor neural networks, *Phys. Rev. Lett.* **124**, 048302 (2019).
- [37] N. Pashine, D. Hexner, A. J. Liu, and S. R. Nagel, Directed aging, memory, and nature's greed, *Science advances* **5**, eaax4215 (2019).
- [38] N. C. Keim, J. D. Paulsen, Z. Zeravcic, S. Sastry, and S. R. Nagel, Memory formation in matter, *Reviews of Modern Physics* **91**, 035002 (2019).